RESPONSE DETERMINATIONS OF COMPTEL FROM CALIBRATION MEASUREMENTS, MODELS, AND SIMULATIONS

R. Diehl [1], H. Aarts [2], K. Bennett [4], W. Collmar [1], H. deBoer [2], A.J.M. Deerenberg [2], J.W. den Herder [2], C. deVries [2], W. Hermsen [2], M. Kippen [3], J. Knödlseder [1], L. Kuiper [2], G.G. Lichti [1], J.A. Lockwood [3], J. Macri [3], M. McConnell [3], R. Much [1], D. Morris [3], J. Ryan [3], V. Schönfelder [1], G. Simpson [3], H. Steinle [1], A.W. Strong [1], B.N. Swanenburg [2], T. van Sant [1], W.R. Webber [3], C. Winkler [4]

[1] Max Planck Institut für Extraterrestrische Physik D-8046 Garching, FRG
[2] Space Research Leiden, Huygens Laboratorium, NL-2333 Leiden, NL
[3] Space Science Center of University of New Hampshire Durham, N.H, USA
[4] ESA/ESTEC Space Science Department NL-2200 Noordwijk, N.L.

INTRODUCTION

The COMPTEL telescope onboard the NASA Gamma Ray Observatory is an instrument with imaging properties quite different from telescopes at longer wavelengths: Focusing of the incoming radiation is impossible due to the penetrating power of the gamma ray photons, the photons rather interact with the electrons and nuclei of the detector material in a particle-like manner. This affects the way the response of the instrument is described, determined, and used. The instrument consists of 2 planes of detector modules, which measure a photon via two consecutive interactions of probabilistic nature: a Compton scatter in the upper detector plane ('D_1'), and an absorption in the lower detector plane ('D_2') (see figure 1). The active scintillation detectors are surrounded by plastic anticoincidence detector domes to reject events originating from charged particles. Background events are suppressed by measurement of the pulse shape of the scintillation light flash in the upper detectors, and by measurement of the time of flight of the scattered photon from upper to lower detector plane.

The instrument electronics records a set of parameters per each event triggering the active telescope detectors in the desired coincidence criteria; these data are transmitted to ground to be binned into measured data arrays and to be deconvolved using appropriate instrument response matrices.

A detailed description of the instrument can be found in (1). In this paper we describe the methods that have been applied by the COMPTEL Collaboration to determine the instrument response matrices; also the resulting instrument response characteristics are summarized.

INSTRUMENT RESPONSE DESCRIPTION

Ideal Instrument Response

The response of the instrument is defined as the distribution of measured event parameter values for incident photons of specific energy and direction:

$$R = R\left(p_{(\text{measured})} \mid p_{(\text{input})} \right)$$

Data Analysis in Astronomy IV, Edited by V. Di Gesù *et al.*
Plenum Press, New York, 1992

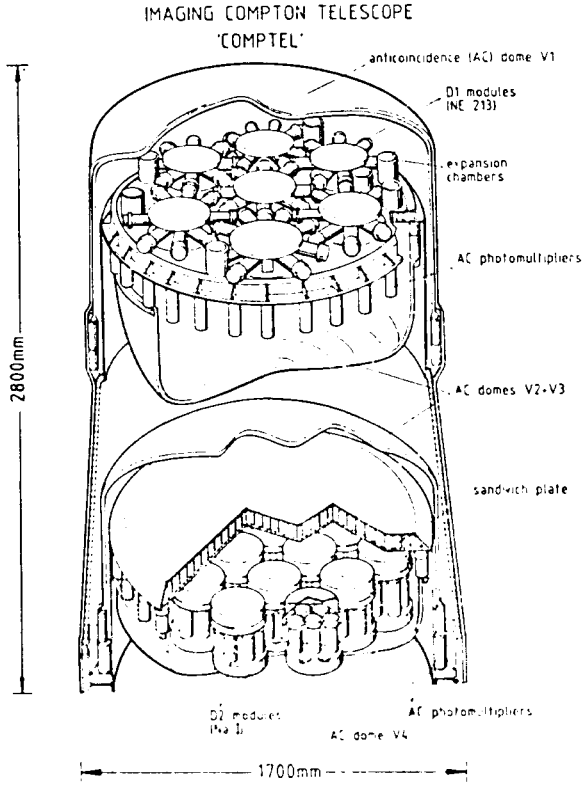

Fig.1. Schematic diagram of the COMPTEL instrument.

The instrument measures directly 21 values per detected photon:
- pulseheights of the set of photomultipliers per D_1 and D_2 module
- detector module identifiers in D_1 and D_2
- time difference between interactions in D_1 and D_2 ('time of flight')
- pulse shape in upper detector module (for neutron event rejection)
- event time and event type flags.

These measurements are converted to the raw event parameters:
- the location of the interactions in both detector planes (measured via the relative signal amplitudes in the set of photomultiplier tubes arranged around the active scintillator volume of a detector cell) $(x_1,y_1,z_1)(x_2,y_2,z_2)$
- the energy deposits of the interactions in both detector subsystems (E_1,E_2)
- secondary event parameters for background signal suppression and sorting (time tag, time-of-flight, pulse shape, event type flags).

As the last set of parameters serves merely for event selections to suppress background events, these are ignored for the discussion of the instrument response due to photon interactions (in this section of the paper).

The interaction location of the 2 successive interactions is determined as exact location within the detector planes. However the symmetry of the instrument components suggests that the response of the individual detector modules in each detector plane is identical: thus the number of event parameters can be reduced by integration over the 2 detector surfaces from 8 to 4, namely:
- two direction angles of the photons on its path from D_1 to D_2 (χ, ψ)
- energy deposit in upper and lower detector module (plane) (E_1,E_2)

The latter two parameters can be converted into the equivalent set of the two parameters "total energy deposit" and "Compton scatter angle", which can be attributed to the physical process of Compton scattering in the instrument more easily:

$$E_{tot} = E_1 + E_2$$

$$\bar{\varphi} = \arccos\left[1 - m_0 c^2 \left(\frac{1}{E_2} - \frac{1}{E_1 + E_2}\right)\right]$$

This yields the response expression:

$$R = R\left(E_{tot}, \bar{\varphi}, \chi, \psi \mid E_\gamma, \alpha, \delta\right)$$

In this representation, the response of an ideal Compton telescope to a beam of monochromatic photons from a specific incidence direction is determined from the Klein Nishina formula for the Compton scatter process as a distribution of scatter angles and scatter directions along a cone-shaped feature in the dataspace spanned by these 3 angles (see figure 2). The cone opening half angle is 45 degrees, as the angular distance of the scattered photon's direction from the source direction is identical to the Compton scatter angle in the ideal case; the cone apex is the direction of the incident photon beam. 'Ideal Compton telescope' here means that all photon interactions are Compton scatters in upper detector plane with totally absorbed scattered photons in the lower detector plane.

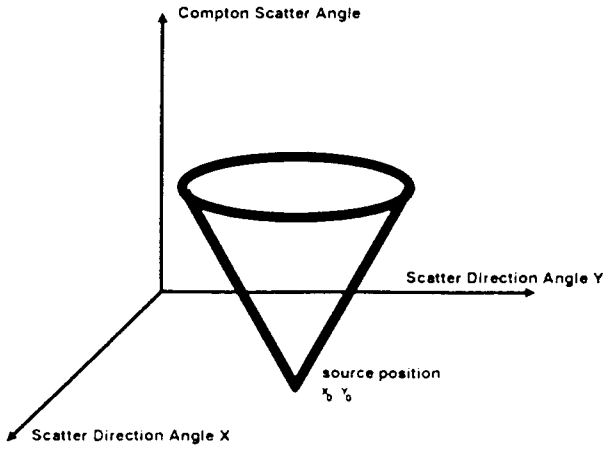

Fig.2. Schematic diagram of the COMPTEL spatial response in the dataspace spanned by scatter direction angles (χ, ψ) and scatter angle φ. The cone apex is the source direction. The blurring due to measurement imperfections widens the cone as a whole, the energy thresholds cut the tip of the cone at the bottom.

Blurring of Instrument Response

In the real situation, imperfections in the location and energy measurements of the interactions, as well as contributions from other (secondary, non-Compton) types of interaction processes result in a broadened distribution of measured event parameters around this ideal cone - we call this the 'point spread function' of the real Compton telescope, as the sharp conelike feature of an ideal point source is spread out by the imperfect measurements of event location and energies.

The blurring components of the response of the Compton telescope are illustrated in figures 3-5:

1) the scintillation detectors of upper and lower plane reveal different measured energy responses to incident photons of specific energy E_γ, due to their different thicknesses for gamma rays:
   - the D_1 NE213A detectors normally show a Compton type of spectrum of measured energy deposits for a monochromatic photon input, as the primary interaction of gamma rays with the detector material is a single Compton scatter interaction with escape of the scattered photon from the detector material. As the scatter angles in the

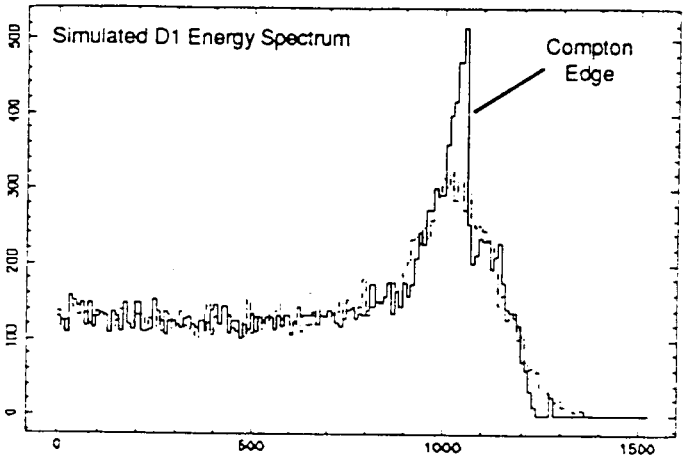

Fig.3a. Energy deposit spectrum as resulting from monochromatic photons at 1.3 MeV (without any additional coincidence requirements) (simulated data)

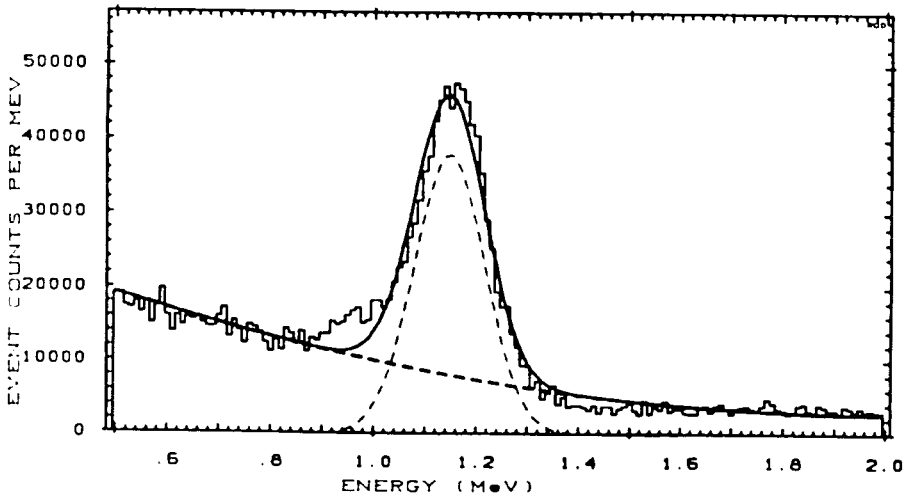

Fig.3b. Response measurement of D_1 detector to a specific energy deposit from a scattering process at a specific scatter angle ('backscatter arrangement', see figure 6b)

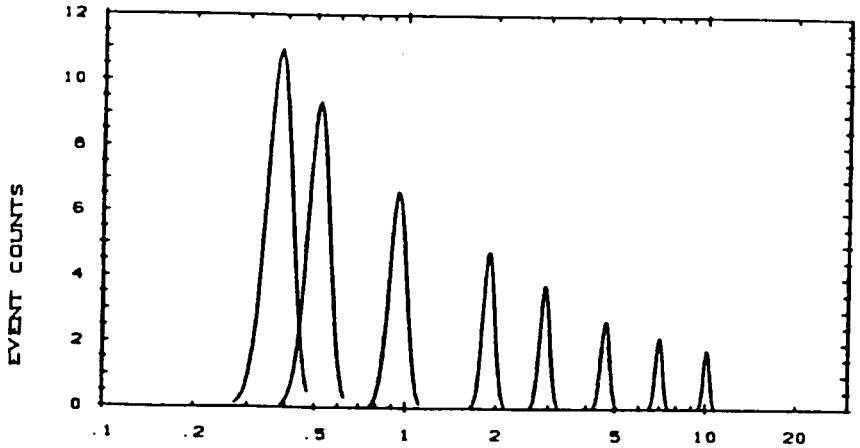

Fig.3c. Response of D_1 detector as a function of input energy (interpolated response model as determined from calibration source energy measurements)

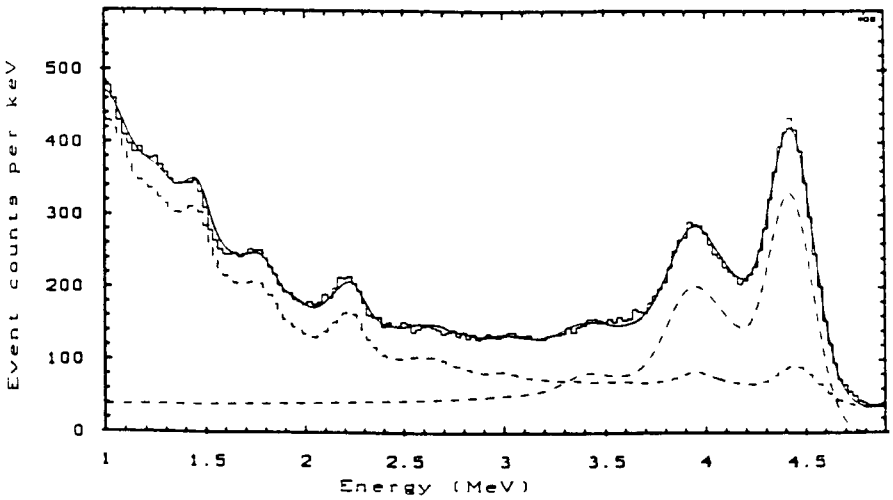

Fig.4a. Energy deposit spectrum of D_2 detector as resulting from monochromatic photons at 4.4 MeV superimposed onto room background: the components from photopeak, escape peaks, and Compton tail are indicated

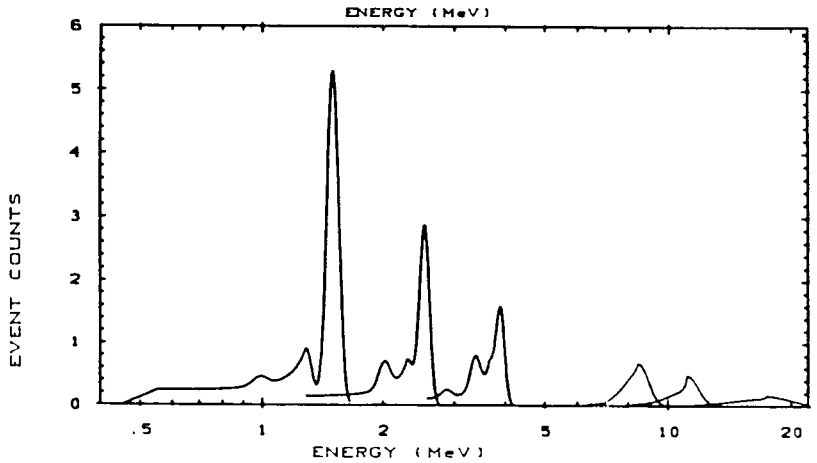

Fig.4b. Response of D_2 detector as a function of input energy (interpolated response model as determined from calibration source energy measurements)

Compton process cover the full range from small angle forward scattering to backward scattering, the measured energy deposits vary from very small energies of a few KeV to the maximum energy deposit for backscattering, the 'Compton edge' energy (example of D_1 energy deposit spectrum see figure 3);
the D_2 NaI detectors have a thickness to gamma rays which results in a series of interactions such as Compton scatterings, pair creation processes in the Coulomb field of detector material nuclei, and photoelectron ejection processes in the shell of these nuclei: as a result of this, at least at low energies the probability of depositing the total energy of the photon within the detector is quite large, resulting in a dominating 'photopeak' in the spectrum of measured energies (see figure 3c). The tail in the spectrum of measured energies is composed from interaction events where the Compton scattered photon escapes the detector ('Compton tail'), or where one ore more of the annihilation photons created as a result of electron-positron pai production interaction escapes the detector ('escape peaks' of first or higher orders, at energies of n *0.511 MeV below the photopeak energy). (example of D_2 energy deposit spectrum see figure 4a; the charateristic components of the spectrum are indicated).
The electronics measuring the scintillation light requires a certain minimum pulse height - this results in an effective energy measurement threshold (about 40 KeV in D_1 and 500 KeV in D_2).. The thresholds are not sharp energy values due to the electronic

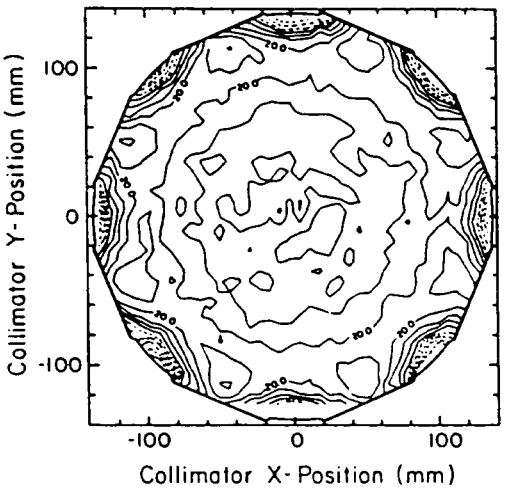

Fig.5a. Interaction location accuracy for D_1 detector modules; photomultiplier tubes are indicated with thick lines; (the 1.7 cm contour line is marked)

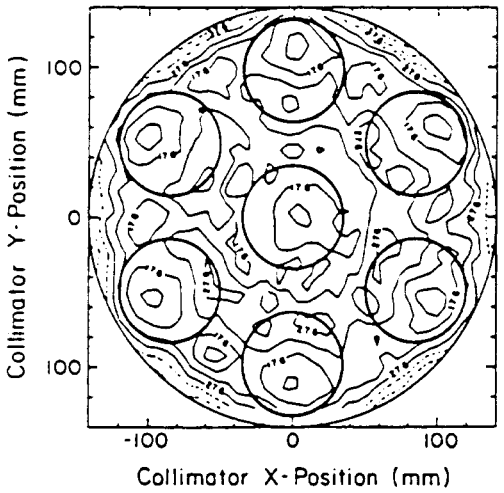

Fig.5b. Interaction location accuracy for D_2 detector modules; photomultiplier tubes are indicated with thick lines circles; (the 1.7 cm contour line is marked)

noise superimposed on the pulseheight signal; this results in rather broad threshold transition regions, on the order of 10 KeV for D_1 and 100 KeV for D_2.

2) the scintillation detector modules of COMPTEL employ the principle of the Anger camera to locate the interaction position within the module. This method is based on a measurement of the scintillation light within a detector by a set of photomultiplier tubes arranged at the detector outer housing; the different distances of the scintillation flash to

the different photomultipliers results in relative signal amplitudes that can be converted into information about the location of the scintillation flash within the detector module. The response of the photyomultiplier sets to photons incident at specific locations of the detector modules was calibrated with a radioactive source located in a massive lead collimator which formed a 'pencil beam' of 1.3. MeV photons with 5 mm beam diameter. The location algorithm to determine event locations from relative signal amplitudes is based on a neural net method. For details of the Anger camera response and determination of the interaction locations see A. Connors et al., this volume. Figure 5 displays the location characteristics that are achieved with this method. The blurring attributed to this interaction location measurement of COMPTEL has been determined to be 2.0-2.6 cm (σ-value for an assumed Gaussian spread of derived locations around the true location) for D_1 modules at 1 MeV, and 0.5-2.5 cm for D_2 modules at 1.27 MeV.

The spatial response (imaging response) of the telescope is derived for intervals of measured energy deposits E_{tot} as a distribution as a distribution in the 3 'spatial dataspace' coordinates (χ, ψ, $\bar{\varphi}$) for the specified spatial photons incidence ection direction coordinates (χ_0 ,ψ_0) of photons with specific energy Egamma.

The spectral response (energy response) of the telescope is derived for regions of spatial dataspace parameters (χ, ψ, $\bar{\varphi}$) as a distribution in measured energies E_{tot} for specified energy E_γ of the input photon.

The response of the instrument is used in the analysis of instrument data via a deconvolution of measured event distributions to derive a distribution of parameters for incoming photons (see e.g. discussion of the 'Maximum Entropy' deconvolution by Strong et al., this volume). This response must be determined independently prior to data analysis via calibration measurements and simulations.

INSTRUMENT RESPONSE DETERMINATION AND RESULTS

There are 3 independent (but related) ways to determine the instrument response:

1) calibration measurements of instrument data for know monochromatic photon sources at specified positions within the instrument field of view
2) calibration measurements of instrument detector module data for know monochromatic photon sources, and composition of these detector module responses to a telescope response via (assumed) physical characteristics of the telescope
3) simulation of the instrument detector module physical processes that are experienced by interacting photons.

All 3 response determination methods have their distinct advantages and disadvantages, and are compared in the following.

The COMPTEL response determination was based on a combination of the above approaches:

- The responses of the upper and lower detector modules were calibrated at photon energies from 0.3 to20 MeV
- The telescope was irradiated with photon sources at a range of incidence angles, also testing (and utilizing) instrumental symmetries
- Photon interaction computer software from high energy nuclear physics laboratories was adapted to theCOMPTEL instrument to generate simulated event messages.

Response Calibration of Telescope

This appears to be the straight forward measurement of the real instrument response to photons of specified incoming energy and direction. In reality, calibration measurements suffer from imperfections, however, which one wishes to not directly degrade the accuracy of the response knowledge. Such imperfections are e.g.:

- non-monochromatic photon sources (more than one gamma ray line emitted by various calibration sources)
- background photon sources, the contribution of which cannot accurately be assessed; background subtractions are affected by the background measurement statistics and sometimes yield 'negative counts' in some bins.
- calibration photon source position notcharacteristic for the photon source position during the real measurement (e.g. not at virtually infinite distance)
- calibration photon sources only available at a few energies.

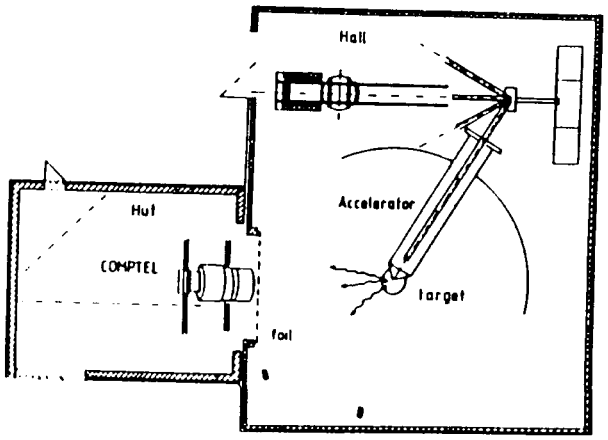

Fig.6a. Experiment setup at GSF Neuherberg accelerator facility; the calibration photons are generated in a target at the end of the beam pipe in the center of the experiment hall; COMPTEL is mounted on the 2 axis-rotation capable dolly in the attached experiment hall

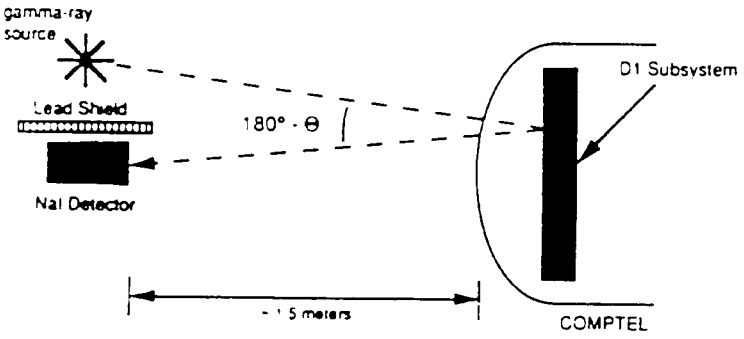

Fig.6b. Backscatter setup for calibration of the D_1 response with radioactive sources

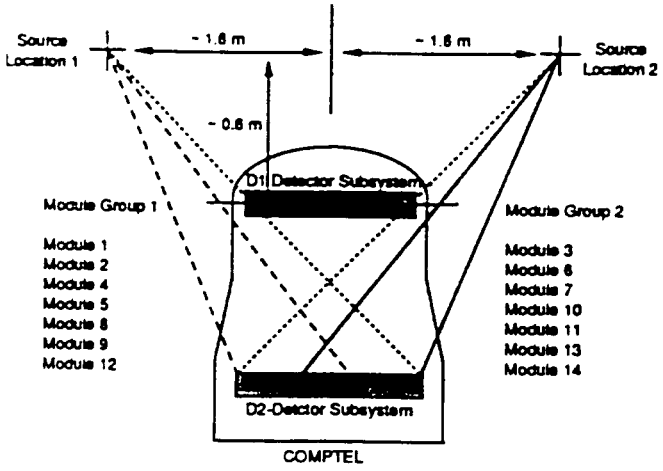

Fig.6c. Setup for calibration of the D_2 response with radioactive sources

In summer 1987 the telescope manufacturing was complete, and the flight instrument was mounted in a special experiment hall at the accelerator site onto a calibration dolly which allowed manipulation of the instrument such as to position the photon generating target of the accelerator beam pipe in any position within the telescope field of view (see figure 6). Radioactive sources were also used for calibration, they were mounted at the backside of the reaction target in order to have a compatible setup and local background environment. The calibrated energies and positions were:

Source	Energy	Zenith Angles
Mn^{54}	0.84	0 / 20 / 40* / 60
Na^{22}	1.27	0 / 10* / 20 / 40 / 60* / 80 / 102
Na^{24}	2.75	0 / 10* / 20* / 30 / 40 / 60*
Am^{241}/Be^{9}	4.43	0 / 10* / 20 / 40 / 60
O^{16}	6.13	0 / 5 / 10* / 15 / 20* / 30 / 40* / 50 / 60
C^{12}	12.14	0 / 5 / 10* / 15 / 20 / 30 / 40* / 102
Tritium	20.25	0 / 15* / 40

* At these zenith angles, more than one azimuthal orientation of the instrument was calibrated

Alltogether about the equivalent of 1.5 years of mission data were recorded in the 2 month calibration activity, before the telescope was shipped to the GRO satellite manufacturer for integration onto the observatory together with the 3 other GRO instruments.

The results of the instrument response as a whole are presented in figure 7 (spectral response) and figure 9-10 (imaging response) for different energies. It is noted that the response measurements at energies above 10 MeV suffer from the difficulties to provide clean monochromatic photon sources from nuclear reactions at an intensity which guarantees a satisfactory signal-to-noise ratio for the calibration data.

Response Calibration for Telescope Components

This approach makes use of calibration measurements and known instrument characteristics in a way to avoid the direct impact of calibration inadequacies onto response inaccuracies, however at the price of involving some prior (maybe imperfect) knowledge about the instrument's imaging response. In the COMPTEL Compton scatter telescope, this approach assumes the telescope response to detect an event via the Compton scatter process, where the incoming photon is Compton scattered in the upper detector plane and (approximately) absorbed in the lower detector plane; the instrument response is assumed to be determined mainly by the characteristics of the individual scintillation detector modules, rather than by the characteristics of any process resulting in quasi simultaneous scintillation events in the two detector planes.

The response of the D_1 and D_2 detector components had been calibrated with the experimental setup as shown in figure 6b,c. The setup for D_1 calibration had to introduce an additional coincidence with an external detector to constrain the energy deposit in the module ('backscatter arrangement'). For D_2 response calibration, 2 different source positions were required due to the shadowing effect of the D_1 detector platform.

The assumption of a Compton scatter event in the upper detector plane results in specification of known energy deposit and scatter angle in the upper detector plane from the incoming photon's energy, which is equivalent to known energy deposits in both detector planes as specified by the incoming photon's energy and the interaction positions in both detector planes. From this, one may calculate the telescope response as a result of the individual scintillation detector module responses to specified energy deposits via:

$$\hat{f}\left(\varphi_{geo}, \bar{\varphi}; E_\gamma\right) = \left(1 - e^{-\bar{\tau}\mu\left(\hat{E}_2\left(\varphi_{geo}, E_\gamma\right)\right)}\right) \cdot P\left(\varphi_{geo}; E_\gamma\right) \cdot a\left(\bar{\varphi} \mid \varphi_{geo}; E_\gamma\right)$$

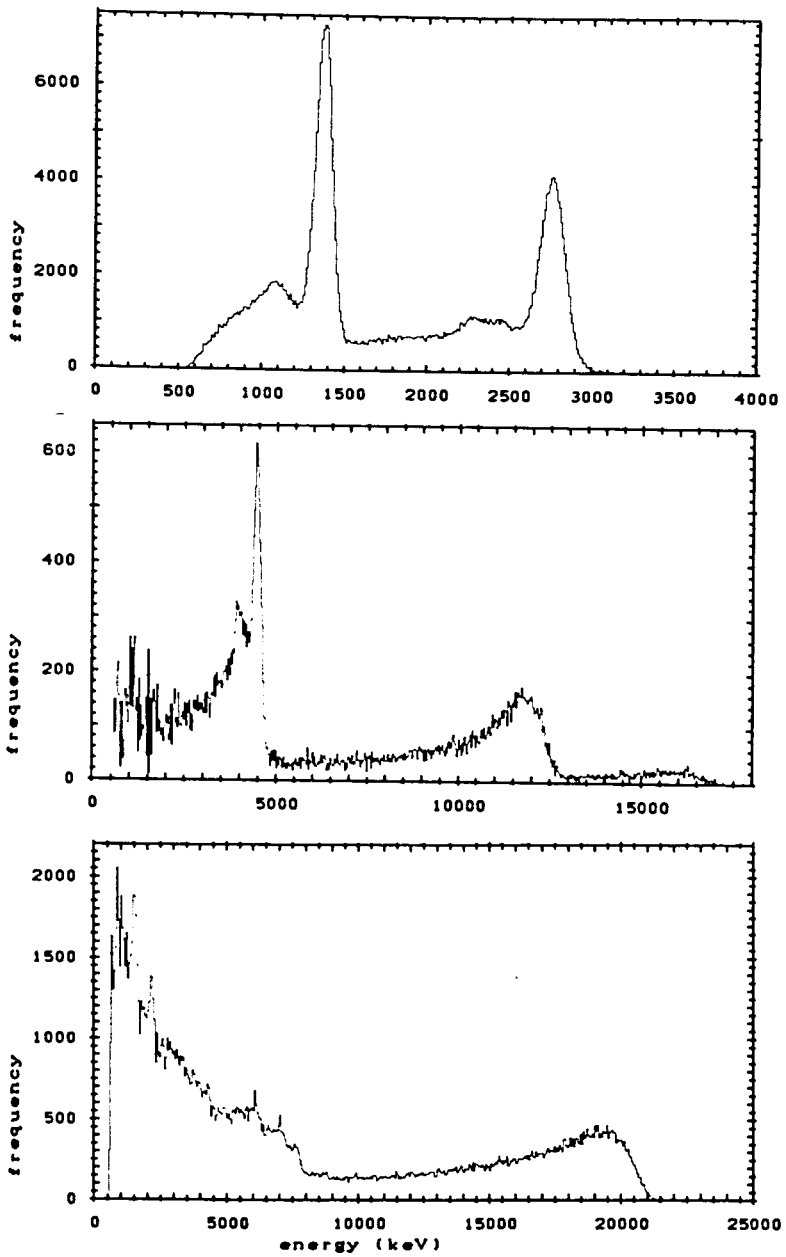

Fig.7. Energy response measurements for the telescope with calibration photons from radioactive ^{24}Na, (1.37 and 2.75 MeV), from the Boron target (12.14, 4.43, and 16.57 MeV) and Tritium target (20.25 MeV) nuclear reactions

as a probability per angular interval in φ_{geo} and $\tilde{\varphi}$. Here 'P' is the probability density of φ_{geo}, which is given by the Klein-Nishina formula, and 'a' is the conditional probability density of $\tilde{\varphi}$ for a given φ_{geo}. $(1 - e^{-\bar{\tau}\mu(\hat{E}_2)})$ is the probability for an interaction in D_2, determined by the average D_2 thickness $\bar{\tau}$ and the interaction coefficient $\mu(\hat{E}_2)$. The essential term is the convolution of the 2 energy responses of the 2 detectors in the regime enclosed by the detector thresholds E_l, E_u:

$$a\left(\bar{\varphi} \mid \varphi_{geo}; E_\gamma\right) = \int_{E^{-}\left(\bar{\varphi}, E_{1,1}, E_{1,2}\right)}^{E^{+}\left(\bar{\varphi}, E_{1,1}, E_{1,2}\right)} g_1\left(E_1 \mid \hat{E}_1\left(E_\gamma, \varphi_{geo}\right)\right)$$

$$\cdot g_2\left(E_2\left(E_1', \bar{\varphi}\right) \mid \hat{E}_2\left(E_\gamma, \varphi_{geo}\right)\right) \cdot J\left(E_1, \bar{\varphi}\right) \cdot dE_1$$

E_2 can be expressed as a function of E_1 and $\bar{\varphi}$:

$$E_2\left(E_1, \bar{\varphi}\right) = -\frac{E_1}{2} + \sqrt{\frac{m_0 c^2}{\sin^2\left(\frac{\bar{\varphi}}{2}\right)} \cdot \frac{E_1}{2} + \left(\frac{E_1}{2}\right)^2}$$

In this approach the calibration measurements of the individual scintillation detector responses are much less critical with respect to the photon source position: background photon radiation can more easily be subtracted, as the characteristics of such scintillation detectors can be fitted by much more reliable models from text books or other laboratory measurements (compared to the complex Compton telescope coincidence instrument's response). The disadvantage of this approach, however, is that non-Compton scatter event types are not represented by the resulting telescope response function. We know that such event types exist and contribute significantly to the instrument response at energies above 10 MeV. Another disadvantage is the empirical inclusion of the interaction location uncertainty as a parameter, with which the calculated PSF is convolved via an assumed Gaussian:

$$f_s\left(\chi, \psi, \bar{\varphi}; E_\gamma\right) = \int_{-\infty}^{\infty}\int_{-\infty}^{\infty} s_x\left(\chi, \chi'\right) s_y\left(\psi, \psi'\right) \cdot \tilde{f}\left(\chi', \psi', \bar{\varphi}; E_\gamma\right) d\psi' d\chi'$$

where

$$s_x\left(\chi, \chi'\right) = \frac{1}{\sqrt{2\pi\lambda\left(E_\gamma, \varphi_{geo}\right)}} e^{\frac{-\left(\chi - \chi'\right)^2}{2\lambda\left(E_\gamma, \varphi_{geo}\right)}}$$

$$s_y\left(\psi, \psi'\right) = \frac{1}{\sqrt{2\pi\lambda\left(E_\gamma, \varphi_{geo}\right)}} e^{\frac{-\left(\psi - \psi'\right)^2}{2\lambda\left(E_\gamma, \varphi_{geo}\right)}}$$

is the function of the scatter direction uncertainty due to the imperfect positional resolution of the interaction location in D_1 and D_2, which is convolved with the $\bar{\varphi}$ response (characterized by the energy resolution in D_1 and D_2).

The final conversion of this model to yield the 3-dimensional model in spatial dataspace is:

$$\tilde{f}\left(\chi, \psi, \bar{\varphi}; E_\gamma\right) = \hat{f}\left(\varphi_{geo}\left(\chi, \psi\right), \bar{\varphi}; E_\gamma\right) \cdot \frac{\hat{\Delta\Omega}}{\tilde{\Delta\Omega}}$$

where the discrepancy between spherical and radial grid is taken into account via the solid angle weighting.

The response of scintillation detectors (both organic scintillation detectors with NE213 as active material, as well as NaI scintillators) is quite well known from previous measurements and literature. Therefore the measurements of the COMPTEL detector modules can be fitted with significant prior knowledge/good models, such that the impact of the particular detector module geometries are calibrated to precision. Nevertheless, also in this case the high energy regime above 10 MeV presents problems, with significant uncertainty of the response details at these energies (see figures 3 for D_1 and 4 for D_2)

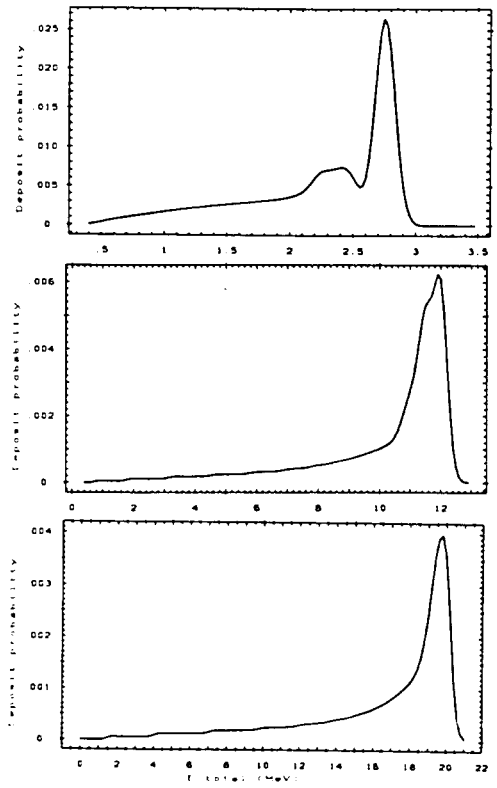

Fig.8a. Energy response as modelled from single detector characteristics, evaluated at energies similar to the telescope calibration energy measurements shown in figure 7

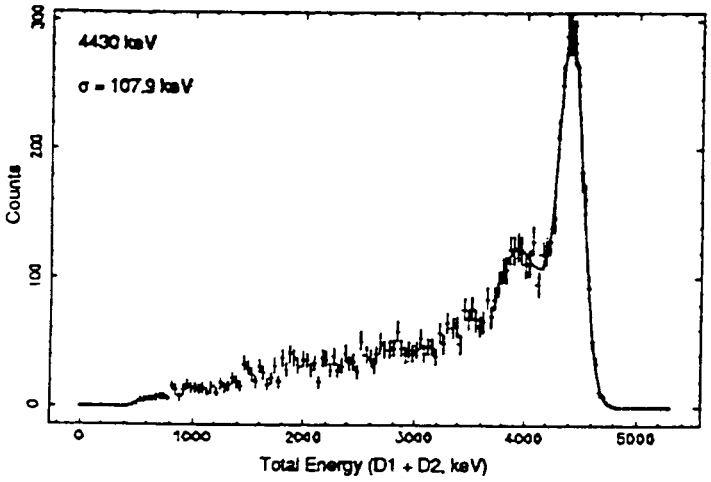

Fig.8b. Energy response as simulated from assumed incidence of 4.4 MeV photons at 10 degrees incidence angle

The telescope response derived from these detector characteristics can be seen from the modelled energy response (see figure 8a) and the 'point spread functions' dispayed in figures 9b and 10. The measured responses in energy domain (figure 7) and point spread function (figure 9a) show similar features, although in detail the distributions are more erratic and broader in the telescope run measurements. The 2-dimensional PSF's cannot directly be compared, as the modelled PSF does not contain the contribution from location uncertainty

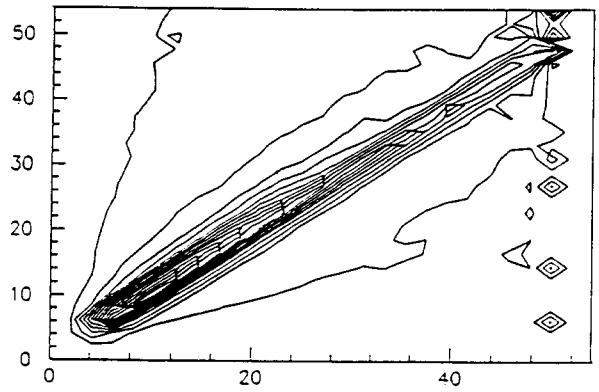

Fig.9a. Imaging response from telescope calibration measurement at 6.13 MeV

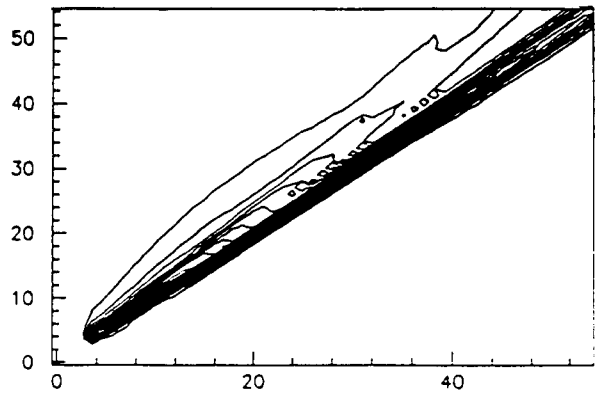

Fig.9b. Imaging response from modelling based on single detector characteristics, at 6.13 MeV. This response does not contain yet the effect of interaction location smearing, therefore it appears sharper than the measured response

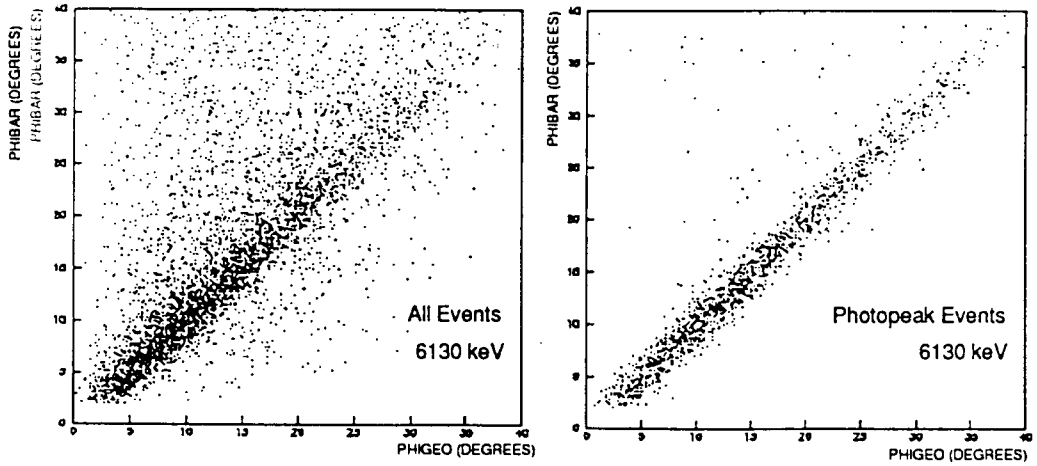

Fig.9c. Imaging response from simulations of the telescope with different selections (6.13 MeV incident photons)

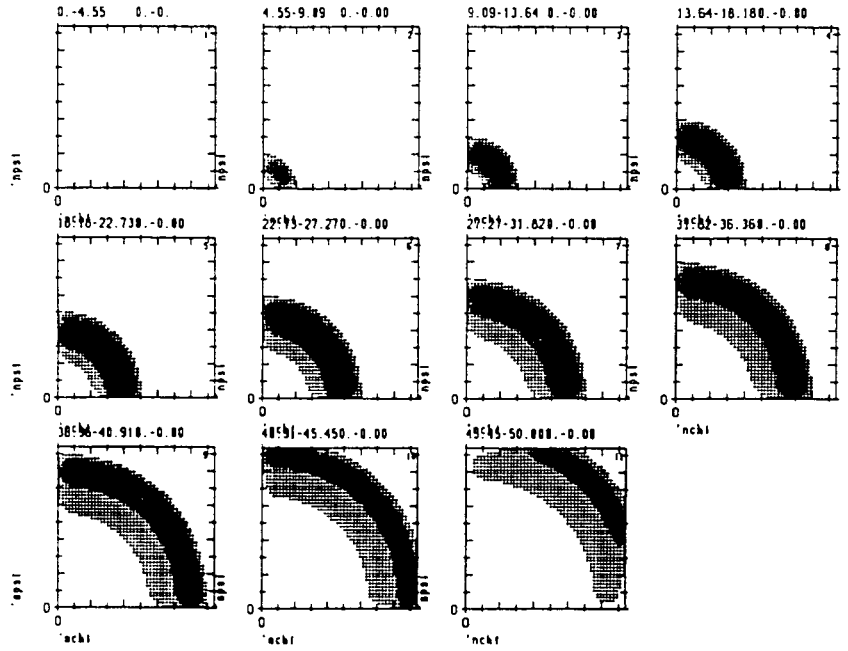

Fig.10. Imaging response in 3-dimensional dataspace; this matrix represents the point spread function assembling all blurring components of an image in COMPTEL data. It is based on the model response shown in figure 9 center, with an assumed (worst case) location broadening of 2 degrees

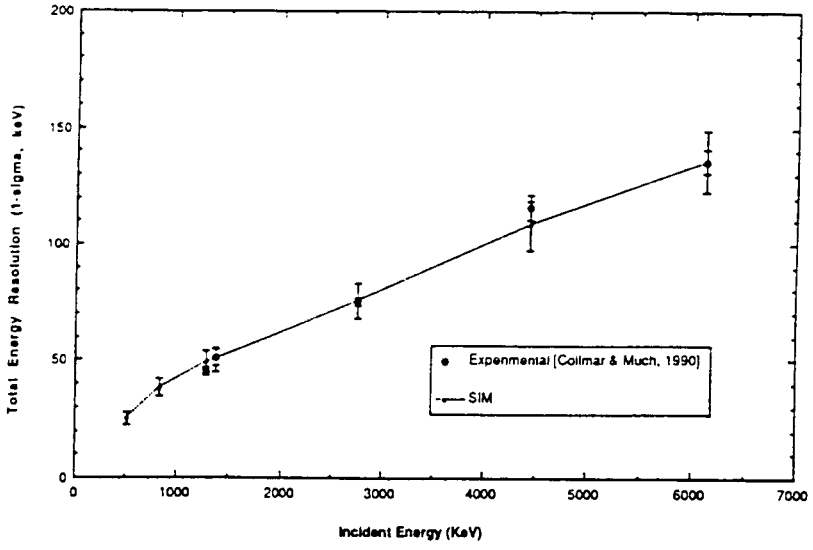

Fig.11. Telescope energy resolution summary (as determined from calibrations and simulations)

yet: rather, the differences in this case point to a contribution to blurring from the location uncertainty of about 1 degree. The 3-dimensional response displayed in figure 10 shows the cone-like feature of the spatial response, and the sidelobes due to incomplete photon absorption in the lower detector plane as secondary features within the main cone response at larger scatter angles.

Response Simulation

The telescope response can be determined also from a computer simulation of the photon interaction physics in the entire telescope, to as much detail as required by the response accurary. If this can be achieved, the telescope response can be regarded as entirely under-

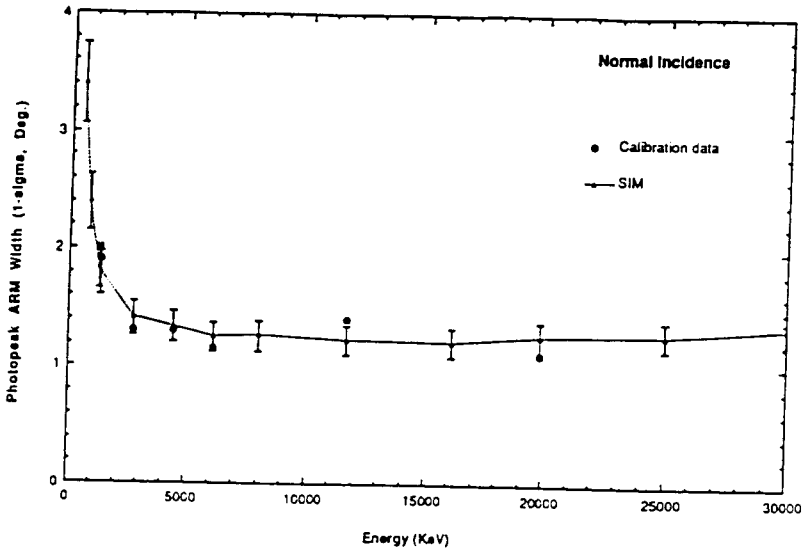

Fig.12. Telescope angular resolution summary (as determined from calibrations and simulations)

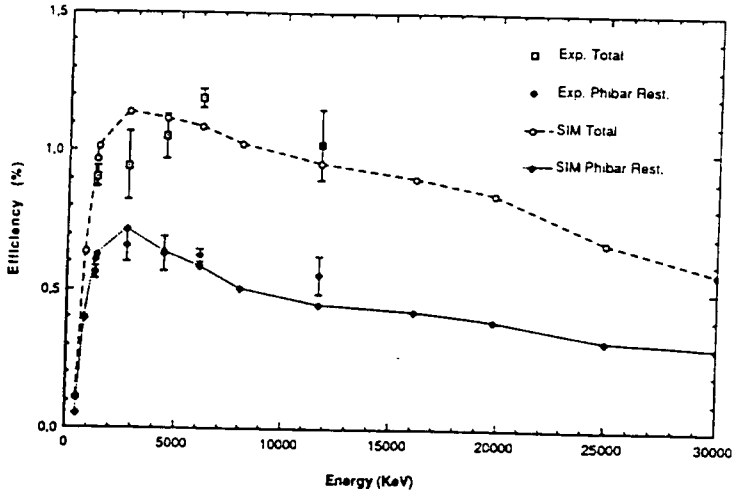

Fig.13. Telescope detection efficiency summary (as determined from calibrations and simulations)

stood. In reality, the simulated data must be compared to calibration measurements of high precision at a large set of photon energies and positions; agreement of simulations with calibrations at many calibration points with the above mentioned caviots provides growing levels of confidence for the simulation software.

The simulation software for COMPTEL is based on the GEANT software package (originating from CERN, Geneva). The instrument geometry had been incorporated, as well as the observed resolution broadening characteristics of the detector modules. We have simulated single detector responses and all calibrated telescope calibration runs at the different angles and energies (see figures 8b and 9c). Comparison of the energy spectra and angular resolution measures confirm the measured values to the expected accuracies; more detailed comparison of point spread functions is done when more statistics is accumulated from simulated event message.

SUMMARY

In conclusion, the spatial response of COMPTEL is available from different approaches, as presented in the figures of this paper. The summary spectral resolution and angular resolution is presented in figures 11 and 12. Figure 13 summarizes the effective area of the telescope as derived from simulations and calibration measurements.

Note that these results are not final yet, as the response determination methods and software are still being optimized, and the simulation database being extended with additional data. Therefore the characteristics presented in this paper document the result status as of the time of the launch of GRO. The final assessment of the optimum approach of response determination is pending. However, the goal of the COMPTEL collaboration is to improve the simulation tools until very accurate agreement with the measurement of the response (both approaches) is assured, as the parameter regime for incoming radiation could not nearly be scanned adequately in the 3 month calibration measurement campaign at theNeuherberg nuclear accelerator facility - COMPTEL's response details will rely on simulation software for a large region of incidence angles and energies.

Meanwhile the observatory had been launched into orbit successfully, and in the initial phase we will determine if the detector characteristics are still the same as at the time of calibration. If the detector response characteristics should have changed, the analysis software allows to fold in updated resolution figures into the response determination tools, so that the in-flight response at the desired angles and energies can be calculated based on calibration, simulation, and in-fligh measurements.

LITERATURE

Schönfelder et al., IEEE Trans Nucl.Sci., NS-31(1), 766 (1984)
Connors et al., this volume (1991)
Strong etal., this volume (1991)
Strong et al., int.resport COM-TN-MPE-K70-53, (1990)
Diehl et al.,NASA Calibration Review (int.report), (1990)
Kippen, Masters Thesis, Univ. of New Hampeshire, USA (1991)